Materials Physics and Mechanics 37 (2018) 34-41 Received: December 22, 2017

MATHEMATICAL AND COMPUTER HOMOGENIZATION MODELS FOR BULK MIXTURE COMPOSITE MATERIALS WITH IMPERFECT INTERFACES

A.A. Nasedkina[1]*, A. Rajagopal[2]

[1]I.I. Vorovich Institute of Mathematics, Mechanics and Computer Sciences, Southern Federal University, Miltchakova Str., 8a, Rostov-on-Don, 344090, Russia

[2]Department of Civil Engineering, Indian Institute of Technology, Hyderabad, 502205, India

*e-mail: nasedkina@math.sfedu.ru

Abstract. The paper describes the homogenization procedure for two-phase mixture elastic composites that consist of two isotropic phases. It is assumed that on the boundary between the phases, special interface boundary conditions are held, where the stress jumps over the interphase boundary are equal to the surface stresses at the interface. Such boundary conditions are used for description of nanoscale effects in elastic nanobodies and nanocomposites. The homogenization problems are solved using the approach of the effective moduli method, the finite element method and the algorithm for generating the representative volume that consists of cubic finite elements with random distribution of element material properties. To provide a numerical example, a wolfram-copper composite is considered, where the interface conditions are modeled by surface membrane elements.

Keywords: composite materials; homogenization problems; effective moduli method; finite element method.

1. Introduction

The process of producing mixture composites often results in composite structures with loosely adhering phase constituents. For example, this happens while sintering the mixtures of piezoceramic powders with more dense granules. In this case, we obtain mixture composite made of piezoceramic and elastic inclusions, where the interphase boundaries can contain air layers. In addition, multiphase mixture composites can experience detachment of materials of different phases while their exploitation. In this and other cases, it is of interest to consider composite structures with imperfect contact conditions at the interphase boundaries [1].

Popular recent models of nanomechanics with surface or interface effects for the composites with nanoscale inhomogeneities consider the boundary conditions with surface stresses on the boundaries between the phases (see for example reviews [2 – 4]). Thus, in the Gurtin-Murdoch model, the boundaries of a nanoscale body are covered by elastic membranes, in which internal forces are described by the surface stresses. Elastic membranes can be also located inside a compound body on the interphase boundary, which allows modeling the imperfect interface boundaries with stress jumps [5 – 9]. The Gurtin-Murdoch model is also frequently used for simulating elastic nanoscale composites. For example, in [10 – 20] and other works in the framework of the elasticity theory with surface stresses, the mechanical properties of the composites with spherical inclusions, fiber and other composites were investigated. The technique of finite element approximations for elastic

http://dx.doi.org/10.18720/MPM.3712018_5

materials with surface effects and numerical examples was demonstrated in [8, 16, 21 – 26] and others.

For the effective moduli determination, i.e. for the homogenization of the composite structure, this work uses a general approach, based on the use of the effective moduli method (with modifications that take into account additional factors on the interphase boundaries), the simulation of the representative volumes and the finite element method for numerical solution of the homogenization problems [21 – 24].

2. Homogenization procedure for a mixture composite with imperfect interfaces

Let us consider a two-phase composite with nanoscale inclusions. Let V is a representative volume; $V^{(j)}$ are the volumes occupied by separate phases ($j = 1, 2$); $V = V^{(1)} \cup V^{(2)}$; $S = \partial V$ is the external boundary of the volume; S^i is the set of the boundary surfaces of materials with different phases; $\mathbf{n}$ is the vector of the unit normal to the external boundary with respect to the volume of the main material $V^{(1)}$; $\mathbf{x}$ is the radius-vector of a point in a Cartesian coordinate system. Let us assume that the volumes $V^{(1)}$ and $V^{(2)}$ are filled with different isotropic elastic materials. Then into framework of classic static linear elasticity theory, we formulate the following system of equations in the volume V with respect to the components of the displacement vector $u_k = u_k(\mathbf{x})$:

$$\partial_l \sigma_{kl} = 0,\ \sigma_{kl} = \lambda \varepsilon_{mm} \delta_{kl} + 2\mu \varepsilon_{kl},\ \varepsilon_{kl} = (\partial_l u_k + \partial_k u_l)/2, \quad (1)$$

where σ_{kl} are the components of the stress tensor; ε_{kl} are the components of the strain tensor; λ, μ are the Lame's coefficients; $\mu = G$ is also called the shear modulus.

As it is known, an elastic material is described by two independent material moduli. The most frequently used are the Young's modulus E and the Poisson's ratio ν. Then the Lame's coefficients λ, $\mu = G$, the bulk modulus K and the stiffness moduli c_{11}, c_{12}, c_{44} can be expressed in terms of the Young's modulus and the Poisson's ratio by well-known formulae:

$$\lambda = \frac{\nu E}{(1+\nu)(1-2\nu)},\ \mu = G = \frac{E}{2(1+\nu)},\ K = \frac{E}{3(1-2\nu)},\ c_{11} = \lambda + 2\mu,\ c_{12} = \lambda,\ c_{44} = G. \quad (2)$$

For a two-phase medium, these moduli differ for each phase: $E = E^{(j)}$, $\nu = \nu^{(j)}$, and so on for $\mathbf{x} \in V^{(j)}$, $j = 1, 2$.

In accordance with the Gurtin-Murdoch model, we adopt that on the nanoscale interphase boundaries S^i the following condition is held:

$$n_l [\sigma_{kl}] = \partial_l^s \sigma_{kl}^i,\ \mathbf{x} \in S^i, \quad (3)$$

where $[\sigma_{kl}] = \sigma_{kl}^{(1)} - \sigma_{kl}^{(2)}$ is the stress jump over the boundary between the phases; $\partial_l^s = \partial_l - n_l (n_m \partial_m)$ is the surface nabla-operator. Here σ_{kl}^i are the components of the tensor of interface stresses, which are related to the strains by the "interface" Hook's law:

$$\sigma_{kl}^i = \lambda^i \varepsilon_{mm}^i \delta_{kl} + 2\mu^i \varepsilon_{kl}^i,\ \varepsilon_{kl}^i = (\partial_l^s u_k^i + \partial_k^s u_l^i)/2,\ u_k^i = (\delta_{km} - n_k n_m) u_m, \quad (4)$$

where λ^i, μ^i are the Lame's coefficients for the interface. We note that instead of λ^i and μ^i other pairs of moduli can be used to formulate the Hooks's law. For example, we can use E^i and ν^i, through which we can express the Lame's coefficients or elastic stiffness using the expressions similar to the plane stress formulas.

Thus, a two-phase composite, consisting of two isotropic elastic phases with interface boundaries, is characterized by four material moduli, for example, $E^{(1)}$, $\nu^{(1)}$, $E^{(2)}$, $\nu^{(2)}$, E^i

and ν^i. If the representative volume has not a pronounced anisotropy in the components distribution, then a such called "equivalent" homogeneous material will also be isotropic and will be described by only two independent moduli, for example, E^{eff} and ν^{eff}. In order to determine these effective moduli, it is enough to solve only one boundary-value problem (1) – (4) in the representative volume of the composite with the boundary condition ($\varepsilon_0 = \text{const}$)

$$u_k = x_1 \varepsilon_0 \delta_{1k}, \ \mathbf{x} \in S. \tag{5}$$

Then, from the solution of problem (1) – (5) similar to [21 – 24], we can find

$$c_{11}^{\text{eff}} = \left\langle \sigma_{11} \right\rangle / \varepsilon_0, \ c_{12}^{\text{eff}} = \left\langle \sigma_{22} \right\rangle / \varepsilon_0, \tag{6}$$

where the angular brackets denote the averaged by the volume V and by the interface S^i values:

$$< (...) >= \frac{1}{|V|} \left(\int_V (...) dV + \int_{S^i} (...) dS^i \right). \tag{7}$$

To check that the homogenized material is isotropic, we can solve problem (1) – (5), which solution should give: $c_{12}^{\text{eff}} \approx \left\langle \sigma_{33} \right\rangle / \varepsilon_0$; $\left\langle \sigma_{km} \right\rangle \approx 0$, $k \neq m$. For additional control of the quality of the representative volume, it makes sense to solve problem (1) – (4) with a shear boundary condition: $u_k = \varepsilon_0 (x_3 \delta_{2k} + x_2 \delta_{3k}) / 2$, $\mathbf{x} \in S$. If we obtain $c_{44}^{\text{eff}} = \left\langle \sigma_{23} \right\rangle / \varepsilon_0$ from the solution of this problem, then this value should be approximately equal to $c_{44}^{\text{eff}} \approx (c_{11}^{\text{eff}} - c_{12}^{\text{eff}}) / 2$, where the moduli c_{11}^{eff}, c_{12}^{eff} are determined from the solution of the previous problem.

In conclusion of this section, we would like to note that for nanostructured composites taking into account the interface surface effects leads to the appearance of special boundary conditions (3), (4) on the surface S^i and to the necessity of calculating the averaged stresses in (7) not only by the volume V, but also by the surface S^i. In a similar way we can consider the problem of homogenization for the composites with imperfect contacts on S^i, for example, with the interface conditions of spring type [1].

3. Numerical examples

Problem (1) – (5) was numerically solved by the finite element method in the finite element package ANSYS using the technique similar to the one described in [21 – 23]. The representative volume V was chosen in the shape of a cube with the side L, which was evenly divided into smaller geometrically identical cubes. These cubes were eight node hexahedral finite elements SOLID45. As a result, in the volume V there were $n_V = n^3$ finite elements, where n is the number of elements along one of the axis. For the simulation of a two-phase composite, the finite elements had properties of one of the phases. At the beginning, all elements had the properties of the first phase. Then, based on the required percentage of the material of the second phase p_a, for the randomly chosen $n_p = \text{NINT}(n_V p_a / 100)$ finite elements, their material properties were changed to the material properties of the second phase (here NINT is the rounding function to nearest integer in ANSYS APDL programming language). We also note that the resulting percentage of inclusions $p = 100 n_p / n_V$ can differ from the expected value p_a, although this difference is usually negligibly small.

Then the boundaries of the elements with different material properties were automatically [21 – 23] covered by four-node shell elements SHELL63 with the option of

only membrane stresses. At the end all interface edges were covered by membrane elastic finite elements, which simulated the presence of interface stresses (3), (4) on the boundaries S^i. At the next stage, for the generated representative volume, we solved static problem (1) – (5), and after that in ANSYS postprocessor we calculated the averaged stresses by both volume and surface elements. Lastly, using formulae (6), (7) and the obtained averaged stresses, we calculated the effective moduli of the composite, taking into account the interface effects.

We note that for the same size L of the volume V, depending on the number of elements n along the axes, the size $l = L/n$ of finite elements can be different, hence, the size of inclusions can be different. Therefore, for a fixed percentage of inclusions p and increasing n, the size of inclusions will be smaller, but the total number of inclusions n_p will increase, and thus the total area of the boundary S^i will also increase [21 – 23].

To provide an example, we consider the problem of finding the effective moduli of a two-phase composite, where the first (main) phase is wolfram and the second (inclusion) phase is copper. As it is known, both phases can be adopted as isotropic materials. For numerical results, we took the following values of bulk material moduli of the first and second phases: $E^{(1)} = 4 \cdot 10^{11}$ N/m^2; $\nu^{(1)} = 0.28$; $E^{(2)} = 1.1 \cdot 10^{11}$ N/m^2; $\nu^{(2)} = 0.34$. It is easy to note that the material of the first phase is almost 4 times stiffer than the material of the second phase. However, the Poisson's ratio of the material of the first phase is smaller than that of the second phase.

As the interface stresses were simulated by the finite elements of elastic membranes, it was necessary for them to set the thickness h^i. The Young's modulus was taken proportional to the difference between the Young's moduli of two phases $\widetilde{E}^i = k^s (E^{(1)} - E^{(2)})$, where k^s is a dimensionless factor and the Poisson's ratio is determined by the formula $\nu^i = (\nu^{(1)} + \nu^{(2)})/2$. Such approach leads to taking into account the stresses (3), (4) with the Young's modulus $E^i = h^i \widetilde{E}^i = h^i k^s (E^{(1)} - E^{(2)})$, i.e. in this case the values h^i and k^s are not important independently, but their product $h^i k^s$ is important. In connection to this, in further numerical calculations the thickness h^i was fixed, $h^i = 1$ m, and for the analysis of the interface stresses influence only the coefficient k^s varied from 10^{-4} to 1.

Figures 1, 2 show the dependencies of the effective moduli with respect to the factor k^s in the logarithmic scale ($\lg \equiv \log_{10}$): the Young's modulus E^{eff} (Fig. 1*a*), the shear modulus G^{eff} (Fig. 1*b*), the bulk modulus K^{eff} (Fig. 2*a*), and the Poisson's ratio ν^{eff} (Fig. 2*b*). Here the percentage of inclusions (material of the second phase) remains unchanged p = 10 %, and the curves 1, 2, 3, 4 correspond to the values n = 10, n = 20, n = 30, and n = 40, respectively. As we can see, the behaviors of the effective moduli E^{eff}, G^{eff} and K^{eff}, depending on the interface moduli values, qualitatively coincide, but the moduli E^{eff} and G^{eff} increase slightly more rapidly when increasing k^s, and the Young's modulus increases the most rapidly. For $k^s \le 10^{-3}$, the surface effects have only a slight influence on the values of the stiffness moduli. Approximately starting with the values of $k^s \le 10^{-2}$, the stiffness moduli begin to grow quite rapidly. Thus for the fixed percentage of inclusions p = 10 % with increasing n = 10, 20, 30, 40, the size of inclusions decrease, but the number of inclusions and their total area increase. As a result, the interface effects are manifested in a greater extent, and the stiffness moduli (Figs. 1 and 2*a*) increase (curves 1 are located lower than curves 2, curves 2 are located lower than curves 3,and curves 3 are located lower than curves 4). It should be noted that for large values of the interface stiffness moduli, the overall effective stiffness

moduli of composite nanomaterials with interfaces may exceed the moduli of the stiffest phase in the composite. In Figs. 1 and 2*a*, this effect is observed, when the values of the moduli are larger than the moduli of the stiffest material in the composite (dashed lines).

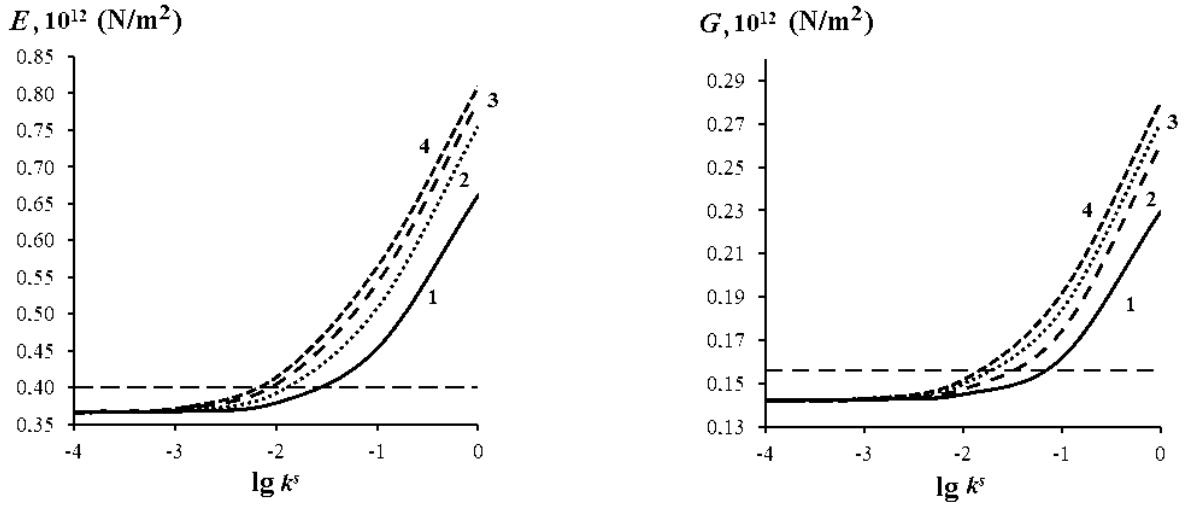

(a) (b)

Fig. 1. Dependencies of the effective moduli E^{eff} (a) and G^{eff} (b) *versus* the factor k^{s} for p = 10 %: curve 1 is for n = 10; curve 2 is for n = 20; curve 3 is for n = 30; curve 4 is for n = 40.

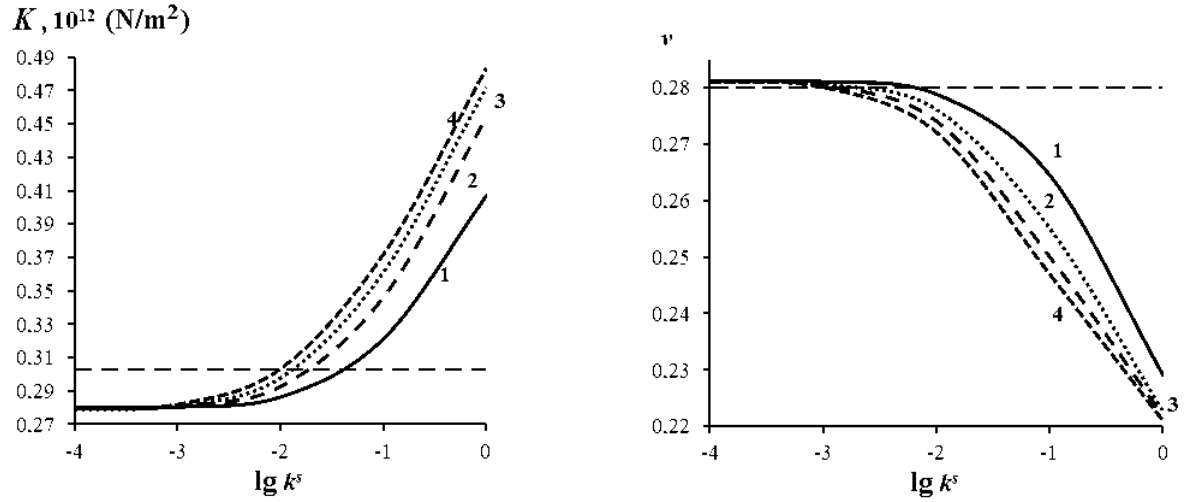

(a) (b)

Fig. 2. Dependencies of the effective moduli K^{eff} (a) and ν^{eff} (b) *versus* the factor k^{s} for p = 10 %: curve 1 is for n = 10; curve 2 is for n = 20; curve 3 is for n = 30; curve 4 is for n = 40.

Figure 2*b* shows that the behavior of the Poisson ratio with increasing interface modulus is opposite to the behavior of the stiffness moduli E^{eff}, G^{eff} and K^{eff}. This can be explained by an increase in the overall stiffness of the material.

In order to analyze the influence of the interface effect on the effective moduli with different percentage of inclusions, we have calculated the effective stiffness moduli with the fixed number of elements n = 20, but with different percentage of inclusions and with

different, but not too large, values of the factor k^s. The results of these calculations are shown in Figs. 3 and 4.

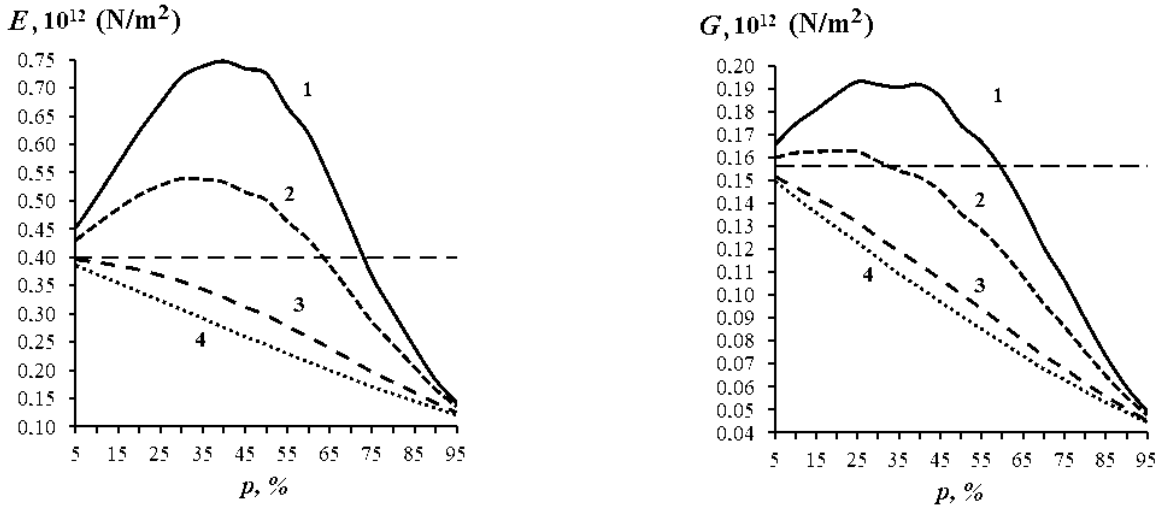

Fig. 3. Dependencies of the effective moduli E^{eff} (a) and G^{eff} (b) *versus* the percentage of inclusions for $n = 20$ and for the factor k^s: curve 1 is for $k^s = 0.1$; curve 2 is for $k^s = 0.05$; curve 3 is for $k^s = 0.01$; curve 4 is for $k^s = 0.001$.

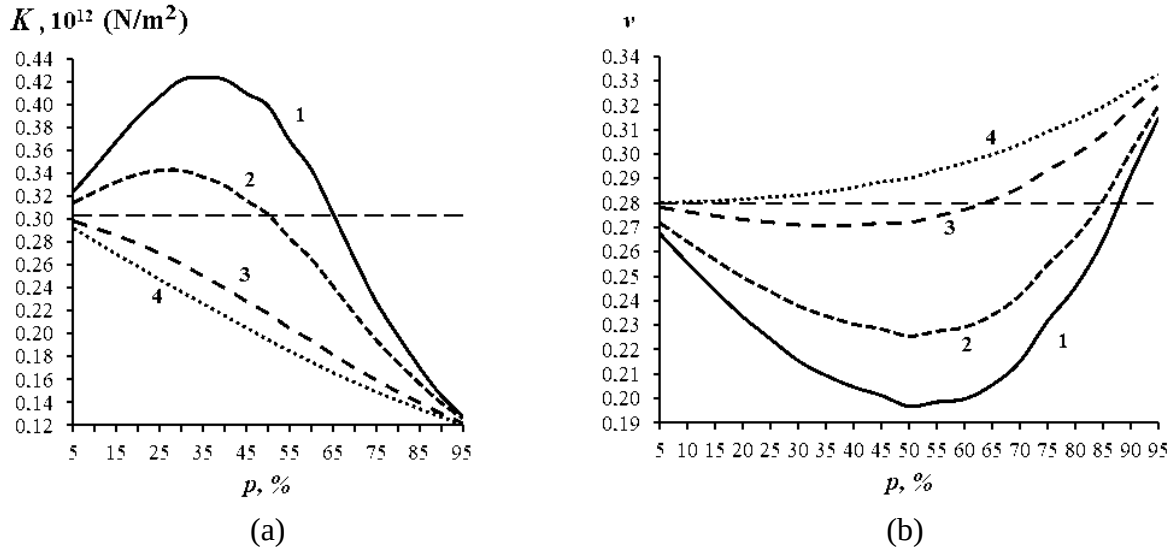

Fig. 4. Dependencies of the effective moduli K^{eff} (a) and ν^{eff} (b) *versus* the percentage of inclusions for $n = 20$ and for the factor k^s: curve 1 is for $k^s = 0.1$; curve 2 is for $k^s = 0.05$; curve 3 is for $k^s = 0.01$; curve 4 is for $k^s = 0.001$.

As these figures demonstrate, for small values of the factor k^s (curves 3 and 4) the interface effects do not affect the stiffness moduli. However, for any percentage of inclusions the interface stresses are larger than the effective stiffness of the composite material. Moreover, as it was mentioned earlier, there are cases when the composite material with interfaces can have greater stiffness than the stiffest material in the composite. This situation

takes place when $k^s = 0.1$ for the Young's modulus E^{eff}, if $p \le 75\%$, for the shear modulus G^{eff}, if $p \le 63\%$, and for the bulk modulus K^{eff}, if $p \le 63\%$, (see curves 1 and 2, which are located higher that the dashed lines in Figs. 3 and 4*a*). When $k^s = 0.05$, the results are more consistent with the experimental data for other materials, and similar situation takes place for the Young's modulus E^{eff}, if $p \le 65\%$, for the shear modulus G^{eff}, if $p \le 33\%$, and for the bulk modulus K^{eff}, if $p \le 50\%$. On the contrary, the Poisson's ratio of the composite structure can be smaller than the Poisson's ratio of the main material for large values of k^s in a wide range of percentage of inclusions *p* (Fig. 4b).

We note that the percentage of softer inclusions and the interface effects have the opposite influence on the effective stiffness: a simple increase of the percentage of softer inclusions leads to a decrease in the stiffness moduli, however, the interface effects increase the stiffness. The growth of the percentage of the softer inclusions for nanocomposite materials with interphase effects entails an increase of the boundaries areas with interface stresses. Therefore, with the increase of the percentage of softer inclusions, the stiffness moduli of nanocomposite materials with interface may increase. For example, for large values of interface moduli an increase of the percentage of inclusions for not very large *p* ($p \le 45\%$ for $k^s = 0.1$ and $p \le 35\%$ for $k^s = 0.05$) leads to a growth of the effective Young's modulus, and with further increase of *p* the effective Young's modulus starts to decrease.

Thus, as it was mentioned in [2, 21 – 24, 27, 28] for porous nanocomposites, from the results of computational experiments the following trends have been observed. If we compare two similar bodies, one with ordinary dimensions and the other with nanoscale dimensions, then for the nanosized body at the expense of surface stresses, the effective stiffness will be greater than for the body of ordinary size. Furthermore, for the composite body with softer inclusions of the macroscopic size and without interfaces, the effective elastic stiffness decreases with an increase of the percentage of inclusions. Meanwhile, for the same percent of inclusions the effective stiffness of the nanocomposite body with softer inclusions and with interface may either decrease or increase depending on the values of the interface moduli, dimensions and number of inclusions. This effect can be explained by the fact that the sizes of the surface interface with interface stresses depend not only on the overall percentage of inclusions, but also on their configuration, size and number.

6. Conclusions

The homogenization model was described for a two-phase elastic composite with surface stresses at the interphase boundaries, which reflected the nanoscale effects for nanostructured composites. This model was applied for the calculation of the effective moduli of a two-phase wolfram-copper composite with interface boundary conditions on the boundaries between the phases. The solutions of the homogenization problems were obtained by the finite element method in ANSYS finite element package for a cubic representative volume with mapped meshing in hexahedral finite elements and random distribution of inclusions. For the considered composite with stiffer skeleton and softer inclusions, we have noted that the effective moduli were dependent on the percentage of inclusions, their configuration and size. These dependencies are similar to known dependencies for nanoporous composites.

Acknowledgements. *This research was performed in the framework of the Russian-Indian RFBR-DST Collaborative project with RFBR grant number 16-58-48009 IND_omi and DST grant number DST/INT/RFBR/IDIR/P-11/2016.*

References

[1] J.M. Baik, R.B. Thompson // *J. Nondestruct. Eval*. **4** (1984) 177.
[2] V.A. Eremeyev // *Acta Mech*. **227** (2016) 29.
[3] J. Wang, Z. Huang, H. Duan, S. Yu, X. Feng, G. Wang, W. Zhang, T. Wang // *Acta Mechanica Solida Sinica* **24(1)** (2011) 52.
[4] K.F. Wang, B.L. Wang, T. Kitamura // *Acta Mech. Sin.* **32(1)** (2016) 83.
[5] G. Chatzigeorgiou, A. Javili, P. Steinmann // *Math. Mech. Solids* **20** (2015) 1130.
[6] G. Chatzigeorgiou, F. Meraghni, A. Javili // *J. Mech. Phys. Solids* **106** (2017) 257.
[7] H.L. Duan, J. Wang, Z.P. Huang, B.L. Karihaloo // *J. Mech. Phys. Solids* **53** (2005) 1574.
[8] A. Javili, P. Steinmann, J. Mosler // *Comput. Methods Appl. Mech. Engrg*. **317** (2017) 274.
[9] H. Le Quang, Q.-C. He // *Mech. Mater*. **40** (2008) 865.
[10] S. Brisard, L. Dormieux, D. Kondo // *Comp. Mater. Sci*. **48** (2010) 589.
[11] S. Brisard, L. Dormieux, D. Kondo // *Comp. Mater. Sci*. **50** (2010) 403.
[12] T. Chen, G.J. Dvorak, C.C. Yu // *Int. J. Solids Struct*. **44** (2007) 941.
[13] H.L. Duan, J. Wang, Z.P. Huang, B.L. Karihaloo // *Proc. R. Soc. A* **461** (2005) 3335.
[14] H.L. Duan, J. Wang, Z.P. Huang, Z.Y. Luo // *Mech. Mater*. **37** (2005) 723.
[15] H.L. Duan, X. Yi, Z.P. Huang, J. Wang // *Mech. Mater*. **39** (2007) 81.
[16] A. Javili, S. Kaessmair, P. Steinmann // *Comput. Methods Appl. Mech. Engrg*. **275** (2014) 76.
[17] V.I. Kushch, S.G. Mogilevskaya, H.K. Stolarski, S.L. Crouch // *Int. J. Solids Struct*. **50** (2013) 1141.
[18] L. Nazarenko, S. Bargmann, H. Stolarski // *Int. J. Solids Struct*. **51** (2014) 954.
[19] Z. Wang, J. Zhu, X.Y. Jin, W.Q. Chen, C. Zhang // *J. Mech. Phys. Solids* **65** (2014) 138.
[20] J.H. Xiao, Y.L. Xu, F.C. Zhang // *Acta Mechanica* **222(1-2)** (2011) 59.
[21] A.V. Nasedkin, A.S. Kornievsky, In: *Methods of Wave Dynamics and Mechanics of Composites for Analysis of Microstructured Materials and Metamaterials*. Series *Advanced Structured Materials*, ed. by M.A. Sumbatyan (Springer, Singapore, 2017) **59** 107.
[22] A.V. Nasedkin, A.S. Kornievsky // *Computational Continuum Mechanics* **10** (2017) 375 (In Russian).
[23] A.V. Nasedkin, A.A. Nasedkina, A.S. Kornievsky // *AIP Conf. Proc*. **1798** (2017) 020110.
[24] A.V. Nasedkin, A.A. Nasedkina, A.S. Kornievsky. In: *Coupled Problems 2017 – Proc. VII Int. Conf. on Coupled Problems in Science and Engineering, 12-14 June 2017, Rhodes Island, Greece*, ed. by M. Papadrakakis, E. Oñate, B.A. Schrefler (CIMNE, Barcelona, Spain, 2017) 1140.
[25] A. Javili, G. Chatzigeorgiou, A.T. McBride, P. Steinmann, C. Linder // *GAMM-Mitteilunger* **38(2)** (2015) 285.
[26] L. Tian, R.K.N.D. Rajapakse // *Comput. Mater. Sci*. **41** (2007) 44.
[27] H.L. Duan, J. Wang, B.L. Karihaloo, Z.P. Huang // *Acta Materialia* **54** (2006) 2983.
[28] V. Eremeyev, N. Morozov // *Doklady Physics* **55(6)** (2010) 279.